Directed Assembly of Non-equilibrium ABA Triblock Copolymer Morphologies on Nanopatterned Substrates

Shengxiang Ji,[†,*] Umang Nagpal,[‡] Guoliang Liu,[‡] Sean P. Delcambre,[‡] Marcus Müller,[§] Juan J. de Pablo,[‡] and Paul F. Nealey[‡,*]

[†]Key Laboratory of Polymer Ecomaterials, Changchun Institute of Applied Chemistry, Chinese Academy of Sciences, 5625 Renmin Street, Changchun 130022, China, [‡]Department of Chemical and Biological Engineering, University of Wisconsin, 1415 Engineering Drive, Madison, Wisconsin 53706, United States, and [§]Institut für Theoretische Physik, Georg-August Universität, 37073 Göttingen, Germany

ABSTRACT

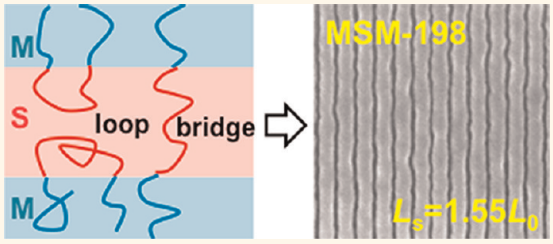

The majority of past work on directed assembly of block copolymers on chemically nanopatterned surfaces (or chemical patterns) has focused on AB diblock copolymers, and the resulting morphologies have generally corresponded to equilibrium states. Here we report a study on directed assembly of ABA triblock copolymers. Directed assembly of thin films of symmetric poly(methyl methacrylate-*b*-styrene-*b*-methyl methacrylate) (PMMA-*b*-PS-*b*-PMMA) triblock copolymers is shown to be capable of achieving a high degree of perfection, registration, and accuracy on striped patterns having periods, L_s, commensurate with the bulk period of the copolymer, L_o. When L_s is incommensurate with L_o, the triblock copolymer domains can reach dimensions up to 55% larger or 13% smaller than L_o. The range over which triblock copolymers tolerate departures from a commensurate L_s is significantly larger than that accessible with the corresponding diblock copolymer material on analogous directed assembly systems. The assembly kinetics of the triblock copolymer is approximately 3 orders of magnitude slower than observed in the diblock system. Theoretically informed simulations are used to interpret our experimental observations; a thermodynamic analysis reveals that triblocks can form highly ordered, non-equilibrium metastable structures that do not arise in the diblock.

KEYWORDS: triblock copolymer · block copolymer lithography · directed assembly · thin film · simulation

Directed assembly of block copolymer films on chemically nanopatterned substrates (or chemical patterns) combines the advantages of traditional photolithography and the ability of block copolymers to self-assemble into ordered structures with characteristic dimensions in the range of tens of nanometers. Recent studies suggest that directed assembly of block copolymers is a promising strategy to create well-defined nanostructures with a high degree of perfection and placement accuracy.[1−20] The resulting block copolymer films have numerous applications, for example, as templates for pattern transfer into underlying substrates for the fabrication of integrated circuits and bit-patterned media.[19−24] Beyond pure block copolymers, past work has also established that block copolymer blends and nanocomposites could also be directed to assemble into nonregular, device-oriented complex geometries on chemical patterns.[6−12,25] More recently, density multiplication was realized by directing the assembly of block copolymer films on chemical patterns with pattern periods, L_s, several times larger than the natural period, L_o, of the copolymer, thereby significantly increasing the resolution of current lithographic tools.[11−20] Past work, however, has largely focused on AB diblock copolymers. In this work, we report results for directed assembly of ABA triblock copolymers on chemical patterns.

The so-called "ABA" triblock copolymers have two identical end "A" blocks covalently bonded to the middle "B" block. The bulk properties of symmetric ABA triblock copolymers have been studied extensively, both theoretically[26−31] and experimentally.[32−34] In the strong segregation regime, ABA triblock copolymers exhibit the same set of morphologies as their analogous AB diblock copolymers.[31,35] Triblocks, however, remain ordered at lower values of the Flory−Huggins interaction parameter; that is, they exhibit lower $(\chi N)_{ODT}$ than the AB diblock copolymer with $N_{AB} = N/2$ monomeric repeat units.[30,36] This attribute makes them potentially attractive for applications because they may assemble into structures with slightly smaller characteristic dimensions than can be

* Address correspondence to sji@ciac.jl.cn, nealey@engr.wisc.edu.

Received for review March 24, 2012 and accepted May 4, 2012.

Published online May 04, 2012
10.1021/nn301306v

achieved by the corresponding AB diblock copolymer. Another useful feature of ABA triblock copolymers is that they exhibit a slightly narrower interfacial width in the weak segregation region than the AB diblock copolymer,[26,29] potentially paving the way toward better control of critical dimensions (CD). Importantly, a distinct difference between triblock and diblock copolymers is that, in triblock copolymers, the central B blocks can form bridges between two different A domains (Figure 1a).[27,28] Bridging conformations in ABA triblock copolymers are believed to significantly improve their bulk mechanical properties[29,32] and, as shown here, also influence their assembly behavior in thin films.

In this work, we use a combination of theoretically informed coarse-grained (TICG) simulations and experiments to examine the assembly behavior of a symmetric triblock copolymer, poly(methyl methacrylate-*b*-styrene-*b*-methyl methacrylate) (MSM-198, M_n = 52-94-52 kg·mol^{-1}), on chemically patterned stripes over a wide range of L_s/L_o. We also compare the assembly behavior of MSM-198 with that of its diblock counterpart, PS-*b*-PMMA (SM-104, M_n = 52-52 kg·mol^{-1}), on the same chemical patterns. SM-104 is chosen because it is effectively one-half of MSM-198 and has a similar L_o to that of MSM-198.

RESULTS AND DISCUSSION

The as-received MSM-198 had a low molecular weight shoulder in the gel permeation chromatography (GPC) trace, indicating the presence of either homopolymer or copolymer impurities. To minimize the effect of impurities on the assembly behavior, MSM-198 was fractionated prior to use. MSM-198 (0.5 g) was first dissolved in THF (5 mL), and methanol (~10 mL) was then added dropwise to the solution while stirring. The solution was kept at 4 °C overnight. The upper layer solution was decanted to remove the lower molecular weight soluble fraction. This purification step was repeated three times to give 0.2 g of purified MSM-198. After three fractionation steps, GPC analysis of the purified MSM-198 showed that the low molecular weight shoulder in the starting MSM-198 was removed and the PDI was reduced from 1.22 to 1.09 (relative to a PS standard, using THF as an eluent). The molar ratio of styrene (S) to methyl methacrylate (MMA) was 1:1.17 by comparing the peak areas of aromatic hydrogens (5H, δ ~6.4−7.2 ppm) in S and the methyl group (3H, δ ~3.7 ppm) in MMA in ^{1}H NMR (Varian UNITY 500 NMR spectrometer) spectra of the purified MSM-198 in $CDCl_3$. L_o of a bulk sample was measured to be 48.5 nm on a Ragaku small-angle X-ray scattering (SAXS) system. The SAXS sample was annealed at 190 °C under vacuum for 60 min and then cooled to room temperature before the data collection.

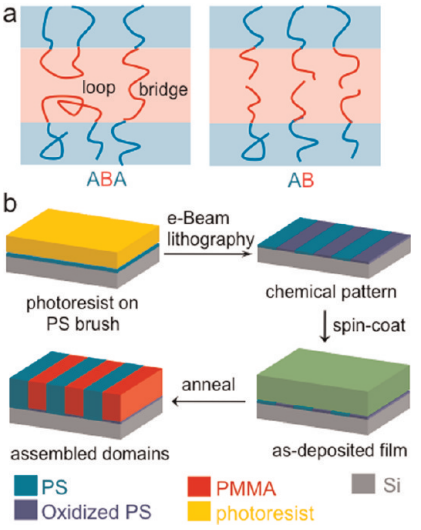

Figure 1. (a) Schematic comparison of ABA triblock and AB diblock copolymers, showing loop and bridge conformations of the molecules. (b) Schematic representation of directed assembly of thin films of block polymers on chemical patterns.

We studied the assembly behavior of MSM-198 on homogeneous nonpreferential (or chemically neutral) surfaces before we directed the assembly of MSM-198 on chemical patterns. The neutral surface was prepared by grafting hydroxyl-terminated poly(styrene-*r*-methyl methacrylate) with 60 mol % of styrene fraction on a silicon substrate.[37] The film thickness was ~50 nm, which is close to the L_o of MSM-198. The assembly was performed at 230 °C for 24 h. A control film of SM-104 was also processed and annealed under the same conditions. MSM-198 had similar assembly behavior to SM-104 on neutral surfaces, and the lamellar domains oriented perpendicular to the substrates in fingerprint-like structures (Figure S1 in Supporting Information).[37−45] The period, L_o, of MSM-198 in thin films on neutral surfaces was measured to be 51.5 nm by Fourier transform analysis of SEM images and was in good agreement with the period measured by SAXS. Close inspection of SEM images in Figure S1 revealed that MSM-198 had an apparent shorter correlation length than SM-104. Analogous to the dependence of the correlation length of block copolymers on the number of blocks in thin films, a similar trend in the decrease of grain sizes with the increase of number of blocks in a block copolymer was also observed in lamellae-forming $(AB)_n$ multiblock copolymers in bulk.[46]

The chemical pattern was fabricated on end-grafted PS brushes by e-beam lithography, and the process is illustrated in Figure 1b.[6] The topographic resist pattern was transformed into a chemical pattern by oxygen plasma treatment. The plasma-modified regions are preferentially wet by PMMA domains; the unmodified PS brush regions are wet by PS domains. The chemical difference of patterned brushes provides the driving force to register the block copolymer microdomains on chemical patterns.

The assembly kinetics of MSM-198 on chemical patterns is approximately 3 orders magnitude slower than that of SM-104. Figure 2a shows SEM images of 50 nm thick films of MSM-198 that were directed to assemble on chemical patterns with L_s = 50 nm at 230 °C for various times. After 1 hour annealing, the copolymer domains oriented perpendicular to the substrate and were partially registered on the chemical patterns with fingerprint-like defect structures or dislocations. The defect density gradually decreased with the increase of the annealing time from 1 to 6 to 12 h. With further increase of the annealing time to 24 h, defect-free assembly of MSM-198 was achieved on the entirely patterned area. In comparison, defect-free assembly of SM-104 on chemical patterns was achieved within 1 min at 230 °C.[5] The assembly kinetics may correlate to the chain mobility that is associated with the molecular weight and chain entanglement. MSM-198 has a higher molecular weight than SM-104; however, the molecular weight difference should not contribute to such a large difference in the assembly kinetics because directed assembly of a diblock PS-*b*-PMMA with M_n = 85−91 kg/mol, close to M_n of MSM-198, was achieved on chemical patterns with L_s = 85 nm at 230 °C within only 5 min. As shown below, a key structural difference between MSM-198 and SM-104 is that the middle blocks of MSM-198 can bridge between two interfaces. The presence of a significant portion of bridging (or looping) configurations and the entanglement of the middle blocks may be the main reason for the slower kinetics for MSM-198.

Theoretically informed coarse-grained (TICG) Monte Carlo (MC) simulations were used to investigate the structure evolution of ABA triblock copolymers on chemical patterns.[47−50] As discussed below, the parameters adopted in our model correspond to SM-104 (in the case of diblocks) or MSM-198 (in the case of triblocks). Past work has shown that with such parameters TICG simulations lead to results in quantitative agreement with experiment. The structures observed for ABA triblocks at intermediate stages of the simulation revealed that the copolymer domains nucleate simultaneously at both interfaces, and that the patterned substrate dominates the film structure in thin films. The domains registered on the chemical patterns near the substrate even within the first ~500 MC steps and propagated toward the film surface with the increase of simulation time (Figure 2b),[48] consistent with prior observations on diblock copolymer systems.[3] The surface structure evolved from random to well-aligned lines registered on the chemical patterns, in agreement with the structural evolution observed experimentally (Figure 2a). Previous studies of the self-assembly of block copolymers on homogeneous surfaces also showed that the substrate effect dominates growth in thin films and that the surface morphology was determined by the substrate patterns.[13,45]

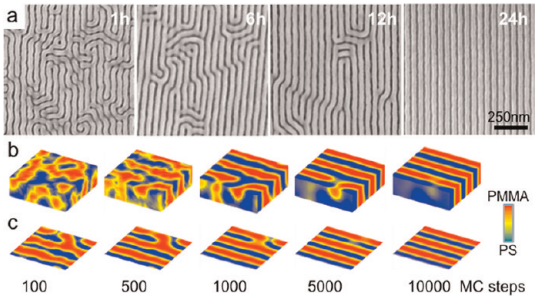

Figure 2. (a) SEM images of 50 nm thick films of MSM-198 that were assembled on chemical patterns with L_s = 50 nm at 230 °C for 1−24 h. Defect-free assembly was achieved when the annealing time was approximately 24 h. The bright and dark stripes are PS and PMMA domains, respectively. The bright stripes are wider than dark stripes due to imaging artifacts. (b) Monte Carlo simulation of MSM-198 on chemical patterns. (c) Slices of the sample near the bottom surface reveal the ordering at the substrate.

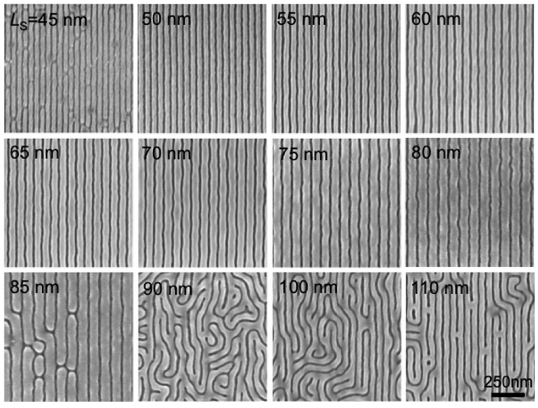

Figure 3. Top-down SEM images of MSM-198 films on chemical patterns with periods of 45−110 nm with a 5 nm increment. Films were annealed at 230 °C for 36 h. MSM-198 expanded up to 55% (80 nm) and contracted less than 13% (45 nm) on chemical patterns in thin films.

A distinct feature of directed assembly of MSM-198 is that MSM-198 can adopt a defect-free lamellar morphology in the presence of chemical patterns with dimensions that are considerably larger (or smaller) than L_s of the underlying chemical patterns. To examine the degree of expansion (or contraction) of MSM-198 domains, we directed the assembly of thin films of MSM-198 on chemical patterns by changing L_s systematically in the range between 45 and 110 nm. Figure 3 shows the corresponding top-down SEM images of 50 nm thick MSM-198 films assembled at 230 °C for 36 h. Defective morphologies, consisting of disconnected domains, were observed in the assembled film on the pattern with L_s = 45 nm, indicating that MSM-198 can no longer assemble on feature sizes that are approximately 13% smaller than L_o, similar to SM-104.[4] Defect-free assembly of MSM-198 was obtained on patterns with L_s = 50−80 nm, with domains registered on underlying patterns and oriented perpendicular to the substrates. We selectively removed PMMA domains by oxygen plasma etching, and the line-edge roughness

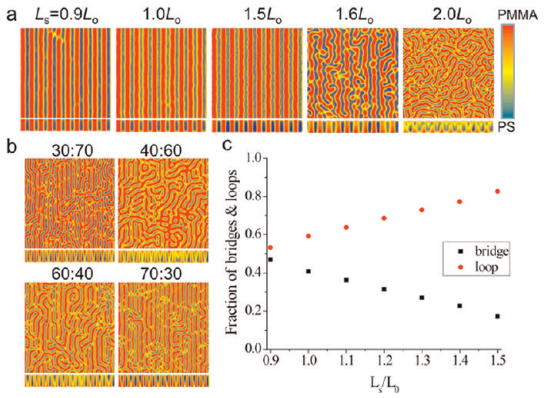

Figure 4. (a) TICG simulations of MSM-198 on chemical patterns with different L_s and 50:50 duty cycle. The 2D top-down (top) and cross-sectional (bottom) color maps are integrated over the *z* direction and computed at depths, *d*, for the top surface ($0 \le d \le 1/8L_z$) to obtain the top-down image. For cross-section images, color maps are integrated over the entire *y* direction. (b) Effect of duty cycle on directed assembly of MSM-198 on chemical patterns with $L_s = 2L_o$. (c) Effect of L_s/L_o on the fraction of bridges and loops on patterns with $L_s = 0.9-1.5L_o$. The fraction of loop conformations increases monotonically with L_s/L_o.

(LER) was calculated from the SEM images (not shown). The 3σ LER of assembled lines gradually increased from 2.6 to 5.2 nm with the increase of L_s from 50 to 80 nm, and wavy line edges were observed in the SEM images of MSM-198 films on 70−80 nm patterns. Defects, such as disconnections and dislocations of domains, were observed on patterns with $L_s = 85$ nm.

Interestingly, these defects show a notable asymmetry, that is, s-shaped jogs and PS lines that simply end, but there are no terminating PMMA lines that are not associated with jogs. This observation is in accord with analytic calculations,[51] indicating that the loop-forming PS block will give rise to a spontaneous curvature toward the PS domain. The MMA block is anchored at the internal interface and bends the interface toward the PS domain in order to enlarge the available volume and reduce the stretching of the block. In the symmetric diblock, this effect is counterbalanced by the PS block such that the net spontaneous curvature of the interface vanishes. In the triblock copolymer, however, some PS blocks form loops; that is, both ends are anchored at the internal interface. Such a loop will pull on the interface, imparting a curvature toward the PS domain, if its two ends are far apart and the loop is stretched. These configurations upset the balance of PS and PMMA blocks and impart a spontaneous curvature and reduced bending rigidity.[51] The latter effect also contributes to the increase of LER upon stretching because stretching increases the loop fraction (see Figure 4c) and concomitantly decreases the bending ridigity of the interfaces.

When the width of the patterns was increased to L_s = 90 nm, the copolymer domains were no longer registered with the underlying chemical pattern, and fingerprint-like structures formed on the film surfaces. Further increase of L_s to 100 and 110 nm resulted in domains that were partially registered to the underlying patterned substrates, forming a structure that combined fingerprint and interpolated line structures with periods of ∼50−55 nm. At $L_s \gg L_o$, the chemical pattern cannot provide sufficient energy for polymer chains to extend and align with the underlying chemical pattern, leading to the formation of fingerprint structures or interpolated line structures. The results shown in Figure 3 indicate that MSM-198 can form ordered, defect-free morphologies on chemical patterns with L_s up to 55% larger than L_o. In comparison, both a diblock copolymer and the ternary blend of a diblock copolymer with 40% homopolymers could only expand ∼10% on chemical patterns.[4,52] On the other hand, both triblock and diblock copolymers could only form defect-free lamellae on chemical patterns with L_s that were ∼10% smaller than their respective L_o.

MC simulations were used to interpret the assembly behavior of MSM-198 on chemical patterns with different L_s. Figure 4a shows top-down and cross-sectional color maps of MSM-198 on chemical patterns with different L_s and 50:50 duty cycles. The copolymer domains are registered on the chemical patterns and are oriented perpendicular to the substrate over a wide range of L_s, from $0.9L_o$ to $1.5L_o$. At $L_s = 1.6L_o$, defects such as necking, dislocation of domains, and even fingerprint-like structures were observed on the film surfaces, in agreement with our experimental observations (Figure 3). At $L_s = 2.0L_o$, registration of the copolymer domains on the chemical patterns near substrates was achieved; however, only fingerprint-like structures formed on the surfaces. In our experiments, coexistence of fingerprint structures and partially aligned interpolated structures was observed. A previous study by Liu *et al.* suggested that perfect density multiplication occurred where the pattern duty cycle and substrate chemistry were optimized.[14] For 2× density multiplication, the perfect duty cycle should be 25:75 or 75:25. Since it is difficult to control the pattern duty cycle under our experimental conditions, we simulated the cases where the duty cycles were 30:70, 40:60, 60:40, and 70:30 (Figure 4b). As expected, 2× density multiplication was observed at a duty cycle of ∼30:70 and 70:30; however, the assembled structures consisted of a mixture of fingerprints and interpolated lines, and perfect density multiplication was not observed.

We calculated the fraction of bridge and loop configurations of MSM-198 on chemical patterns in the range of $L_s = 0.9-1.5L_o$, where directed assembly was achieved. If the chain end-to-end distance of middle blocks was more than the pattern periodicity, it was counted as a bridge, otherwise a loop. The calculation was performed on all chains in the system over 10 000 MC steps to obtain the average number of bridges and loops. Figure 4c shows the bridge and loop fractions as

a function of L_s. Our model predicts that triblock copolymers exhibit 40% of bridge structures in the bulk, in agreement with the percentage (40−45%) predicted by self-consistent field theory by Matsen *et al.*[27,28] On the pattern with $L_s = 1.0L_o$, the percentage of bridges was ~41% (similar to the bulk value). As we increased L_s, the fraction of bridges decreased with L_s; approximately 17% bridge and 83% loop configurations were obtained when $L_s = 1.5L_o$.

In order to examine the thermodynamic stability of lamellar structures as a function of pattern dimensions, we calculated the free energy per chain (ΔF) using thermodynamic integration. If the ΔF *versus* L_s curve was not symmetric around $L_s = L_o$, one could explain the difference between the assembly behaviors of AB and ABA copolymers. One factor that could induce deviations from the symmetric dependence that is observed in AB diblocks is the presence of bridge and loop structures in ABA triblocks; that is, the presence of bridge and loop structures changes the slope of the free-energy curve at $L_s \neq L_o$.[53] For these calculations, we used a system size of $L_x = 16.7L_o$, $L_y = 1.7L_o$, and $L_z = 1L_o$, so that a number of expanded and contracted domains could be accommodated within the same box size. Figure 5 shows the free-energy difference in units of k_BT/chain on chemical patterns with various L_s. The free-energy plot is symmetric and similar to that of the diblock copolymer system, also shown in Figure 5.[2] Such results suggest that the broader, asymmetric range of L_s over which expanded lamellar structures are observed in the triblocks is not due to the thermodynamic compression modulus. For directed assembly, the chemical difference between patterned stripes provides the driving force to directed assembly of block copolymer domains. The driving force should be the same at different pattern periods; however, the experimentally observed assembly behaviors of MSM-198 on chemical patterns with different L_s are not consistent with the symmetric nature of the free-energy plot. These observations therefore lead us to propose that the observed lamellar morphologies at large L_s correspond to kinetically trapped, metastable states.

Simulations were used to explore whether kinetic instead of thermodynamic effects are behind the formation of structures at $L_s \neq L_o$ especially for $L_s > 1.2L_o$. To examine this possibility, the disordered system (with same system size as above) was first allowed to evolve into an ordered structure in the absence of the chemical pattern. Consistent with experiments, we observed a fingerprint structure. This structure was then used as a starting configuration for simulations on chemical patterns, with various values of L_s, in which the morphology was allowed to evolve. We observed that, for $0.9L_o \leq L_s \leq 1.2L_o$, the fingerprint structure evolved into an aligned line structure that was identical to that obtained when a disordered state was used as a

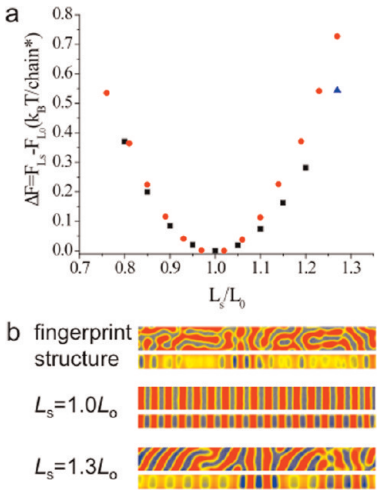

Figure 5. (a) Red circles show the free-energy difference (in k_BT/chain) between perfectly registerd vertical lamellae structures on various pattern periods and perfectly registerd lamellae at $L_s = 1.0L_o$ (red circles). The blue triangle corresponds to the case for $L_s = 1.3L_o$ with unregistered lamellae structures. Also shown with black squares is the free-energy difference for a PS-*b*-PMMA diblock reproduced from Edwards *et al.*[2] and rescaled to match the molecular weight of MSM-198 considered in this work. (b) Top-down (top) and cross-sectional (bottom) images from MC simulations. The fingerprint structure was used as the starting configuration for the simulation of directed assembly on chemical patterns with $L_s = L_o$ and $L_s = 1.3L_o$, for which registered and unregistered lamellae were observed after long production simulation runs, respectively.

starting configuration in Figure 4a. For $L_s > 1.2L_o$, however, we observed that the structures were different than those shown in Figure 4a; for example, for $L_s = 1.3L_o$, we could not arrive at a perfectly registered structure, as illustrated in Figure 5. Free-energy calculations using thermodynamic integration were subsequently used on these disordered structures, and it was found that, for $L_s > 1.2L_o$, their free energy was in fact lower (*i.e.*, they were thermodynamically more stable) than that of morphologies observed when the system is quenched from a disordered state on a chemically patterned susbtrate (as shown in Figure 4), reinforcing the view that the registered lamellar morphologies observed for $L_s > 1.2\ L_o$ (in both experiments and simulations) in fact represent kinetically trapped, non-equilibrium states.

The large expansion ratio, which triblock copolymers are capable of on chemical patterns, could be particularly useful for fabrication of complex structures. For diblock copolymers, block copolymer/homopolymer blends are usually required in order to achieve defect-free structures for blends, jogs, and T-junctions.[6,9,12] To demonstrate some of the unique structural properties of triblock copolymers, we directed the assembly of MSM-198 into "bends", which represent an essential geometry for the fabrication of integrated circuits, and compared it with that of the corresponding diblock copolymer SM-104. For bends with $L_s = 50$ nm, the effective periods at the bend corners (L_c) were 54.1, 70.7, and

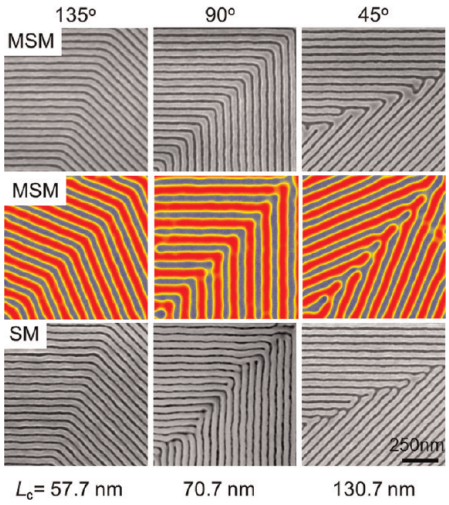

Figure 6. Top-down SEM images of thin films of MSM-198 and SM-104 and images from MC simulations of MSM on chemical patterns with 45, 90, and 135° bend geometries. Films were annealed at 230 °C for 24 h.

130.7 nm for 135, 90, and 45° bends, respectively. Thin films (approximately 50 nm in thickness) of MSM-198 and SM-104 were deposited on two identical chemical patterns and annealed at 230 °C for 24 h under vacuum. Figure 6 shows the corresponding SEM images. Both simulations and experiments show that the triblock can assemble into defect-free domains at corners for bends with 135 and 90° angles; for smaller 45° angles, the domains are disconnected or mismatched. In contrast, for the diblock, dislocations of domains were observed at corners on 90 and 45° bends. The defect structures persisted after annealing times of 3 and 7 days. The effective periods at the corners are significantly larger than the natural periodicity of the materials, and the polymer chains must therefore expand considerably to achieve defect-free assembly. The improved assembly behavior on 90° bends and on patterns with $L_s \neq L_o$ is a result of the surprisingly large expansion ratio of the MSM-198 triblock on chemical patterns.

The film thickness, at which copolymers can be directed to assemble, depends on the strength of chemical patterns and the free energy per volume. Previously, we have demonstrated that we could direct the assembly of cylinder-forming diblock copolymers on chemical patterns with thicknesses up to $\sim 5L_o$. Here we directed the assembly of a 74 nm thick ($\sim 1.44L_o$) film of MSM-198 on chemical patterns with L_s = 50, 55, and 60 nm (Figure 7). Directed assembly on patterns with L_s = 50 and 55 nm was achieved after the sample was annealed at 230 °C for 36 h, but with dislocated domains as defects. On the L_s = 60 nm pattern, directed assembly was possible and the copolymer domains were partially aligned along the pattern direction. When we increased the annealing time to 96 h, the defects disappeared on patterns with L_s = 50 and 55 nm, and wavy lines were found on L_s = 60 nm

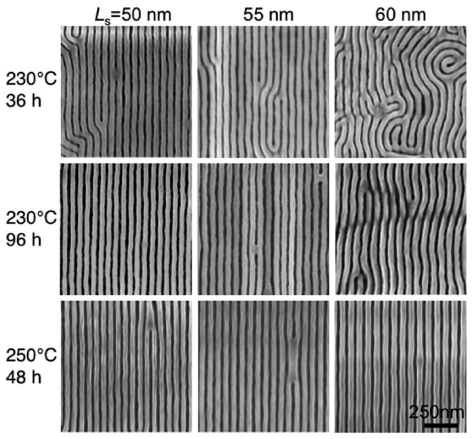

Figure 7. SEM images of 74 nm thick MSM-198 films that were annealed at 230 °C for 36 and 96 h and at 250 °C for 48 h on chemical patterns with L_s = 50−60 nm.

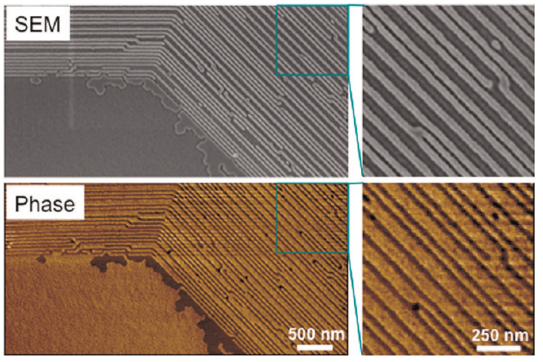

Figure 8. SEM and AFM phase images from the same area in the film of MSM-198 on chemically patterned substrates with W = 0.65 L_s. The brighter domains in SEM and AFM images are from PS and PMMA, respectively.

patterns. When the film was annealed at 250 °C, perfect assembly of MSM-198 on L_s = 60 nm was achieved within 48 h. Further increases of the annealing time or temperature could lead to the directed assembly of even thicker films, but the thermal degradation of the block copolymers becomes a concern.

We observed a unique defect structure in MSM-198 thin films that was directed to assemble on chemical patterns when the width of the wetting stripe (W) was unequal to $0.5L_s$, as shown in Figure 8, in which L_s = 50 nm and $W = 0.65L_s$. The SEM and AFM phase images are from the same area in the assembled MSM-198 thin film. As shown in Figure 8, a significant portion of the bright PS stripes were disconnected but were joined by gray stripes that appeared to be different from the dark PMMA stripes. The AFM phase image in Figure 8 revealed that the gray and dark stripes had the same phase contrasts, indicating that the gray stripes correspond to a layer of PMMA covering a PS domain. The formation of this unique structure may also contribute to the bridging of middle blocks. The middle PS domains registered on the underlying PS. However, because the PS wetting region is significantly wider

than the PMMA wetting region, conservation of mass may result in excess PMMA spreading over PS domains when the film is away from the substrate. In comparison, defect-free assembly of symmetric diblock PS-*b*-PMMA films was obtained on striped patterns with $0.36 \leq W/L_s \leq 0.63$ when $L_s = L_o$.[3]

CONCLUSION

Using a combination of simulations and experiments, we have shown that triblock ABA copolymers of poly(methyl methacrylate-*b*-styrene-*b*-methyl methacrylate) (referred to as MSM-198) can be directed to assemble on chemically patterned substrates with a high degree of registration and perfection. A particularly attractive feature of triblocks is their ability to expand (~55%) and contract (<13%) in thin films when directed to assemble on chemical patterns, which they do by adopting non-equilibrium structures. Such a feature is of interest for fabrication of regular patterns (such as arrays of lines or dots) and irregular patterns (such as bends or jogs), where triblocks are better able to tolerate pattern imperfections and still exhibit defect-free directed assembly without the need to introduce additional components, such as homopolymers or solvents. From a fundamental perspective, the fact that one can reproducibly access non-equilibrium states by introducing patterns on a surface provides intriguing possibilities to further develop our understanding of dynamics and structure formation in nanostructured materials. From a technological point of view, the ability to adopt non-equilibrium states in a controllable manner offers the promise of expanding considerably the palette of morphologies available for nanoscale fabrication.

EXPERIMENTAL SECTION

Materials. Poly(methyl methacrylate-*b*-styrene-*b*-methyl methacrylate) (MSM-198, M_n = 52-94-52 kg·mol^{-1}, polydispersity index (PDI) = 1.22) and PS-*b*-PMMA (M_n = 52-52 and 85-91 kg·mol^{-1}, PDI = 1.07) were purchased from Polymer Source, Inc. PS-OH (M_n = 6 kg·mol^{-1}, PDI = 1.05) was synthesized by anionic polymerization. PMMA photoresist (M_n = 950 kg·mol^{-1}, 4 wt % in chlorobenzene) was purchased from MicroChem, Inc. All solvents were purchased from Aldrich and used as received.

Directed Assembly of Films of Block Copolymers on Lithographically Defined Chemical Patterns. The process to create chemical patterns and direct the assembly of ABA triblock copolymers is shown in Figure 1b. A 40 nm thick PS-OH (6 kg·mol^{-1}) film was deposited on an oxygen-plasma-cleaned silicon substrate by spin-coating from 1 wt % toluene solution and annealed at 160 °C for 24 h under vacuum. Excess PS-OH was removed by sonication in toluene to form a PS brush layer with a thickness of ~4.1 nm. A 50 nm thick PMMA photoresist (950 kg·mol^{-1}) film was deposited onto the PS brush from a 1.2 wt % chlorobenzene solution and baked at 160 °C for 60 s. Striped patterns with periods, L_s, varying from 45 to 110 nm in 5 nm increments and bends with L_s of 50 nm and angles of 135, 90, and 45° were exposed on the resists using electron beam lithography (EBL). EBL was performed on a LEO 1550 VP SEM equipped with a J.C. Nabity pattern generation system with an acceleration voltage of 20 kV. Exposed substrates were developed with a 1:3 (v/v) mixture of methyl isobutyl ketone/isopropyl alcohol for 60 s and rinsed with isopropyl alcohol. The resulting resist pattern was transformed into a chemical pattern on the PS brush by exposing the sample to an oxygen plasma followed by stripping the PMMA photoresist in warm chlorobenzene. Films of MSM-198 and SM-104 were deposited on the chemically patterned substrates by spin-coating from 1.5 wt % toluene solutions, annealed at 230 °C for various times under vacuum, and imaged by SEM with an acceleration voltage of 1 kV.

Monte Carlo Simulations. To explore and differentiate the fundamental structures obtained from block copolymer in bulk and patterned substrates, we use theoretically informed coarse-grained (TICG) Monte Carlo (MC) simulations.[49] The compressibility of the melt, chain connectivity, interactions between monomers, and interactions of the monomers with the substrate are the main properties that govern the copolymer behavior at the mesoscopic length scale relevant to this work. For the triblock at temperature T and confined in a simulation box of volume V, N beads are used to discretize each chain contour. The Hamiltonian H includes contributions from bonded (b), nonbonded (nb), and substrate interactions (s).[54] The bonded energy is described by harmonic springs between adjacent beads of the chains; nonbonded interactions are determined from the local densities, $\Phi_A(r)$ and $\Phi_B(r)$, and substrate interactions are given by an exponentially decaying function of the distance from the surface. The specific functional forms employed in our simulations for such contributions are given by[54]

$$\begin{aligned}\frac{H}{k_BT} &= \frac{H_b[\mathbf{r}_i(s)] + H_{nb}[\Phi_A, \Phi_B] + H_s(\mathbf{r}_i, K)}{k_BT} \\ &= \frac{3}{2}\sum_{s=1}^{N-1}\frac{[\mathbf{r}_i(s+1) - \mathbf{r}_i(s)]^2}{b^2} \\ &\quad + \rho_0\int_v d\mathbf{r}\left[\chi\Phi_A\Phi_B + \frac{\kappa}{2}(1-\Phi_A-\Phi_B)^2\right] \\ &\quad - \frac{\lambda_s^K}{d_s/R_e}\sum_i \exp\left[-\frac{z_i^2}{2d_s^2}\right] \end{aligned} \quad (1)$$

where k_B is the Boltzmann constant, $\mathbf{r}_i(s)$ denotes the Cartesian coordinates of the sth bead in the ith chain, $b = (R_e^2/(N-1))^{1/2}$ is the mean squared bond length, R_e is the mean squared end-to-end distance for an isolated, non-interacting chain, ρ_0 is the average bulk number density of beads, and χ is the Flory–Huggins interaction parameter. Local densities are determined from beads' positions on a grid with spacing $\Delta L = 0.14R_e$.[54] Fluctuations of local density are controlled through a Helfand quadratic approximation (second term of the nonbonded interactions in eq 1)[55] and governed by the finite compressibility κ. For the dense melts considered in this work, the invariant degree of polymerization $\bar{N}$ is proportional to the molecular weight. The coarse-grained parameter R_e sets the length scale for our simulations, and $\sqrt{\bar{N}} = \rho_0 R_e^3/N$, which provides an estimate of the number of chains that interact with any given chain, controls the strength of the fluctuations.[56] For interactions with a patterned substrate, a potential acts on each bead i of type K at position $\mathbf{r}_i$. The potential decays over a short distance $d_s = 0.15R_e$, and it is a function of the normal distance to the substrate, z_i. The parameter $\lambda_s N$ determines the strength of the interaction between beads of type K and the pattern. For simplicity, we assume that, for both PS and PMMA patterned areas, the repulsion for the nonpreferred block is equal in magnitude to the attraction for the preferred block ($\lambda_s^A N = -\lambda_s^B N$).[57] To simulate the chains in a thin film, periodic boundary walls are used in the x and y directions, and two impenetrable hard walls are introduced in the z direction (thickness). For the ABA triblock with molecular weight of 198 kg·mol^{-1} considered in this work, we use $\chi N = 70$, $\kappa N = 96$, $\bar{N} = 170^2$. Each block of the ABA triblock chain is discretized into 8, 16, and

8 beads, respectively. The interaction with the pattern is given by $\lambda_s N = 0.5$. For free-energy calculations, we use thermodynamic integration as used in previous works.[57−59] To simulate different pattern widths, we vary the pattern periodicity, L_s. The dimensions of the simulation box are $L_x \times L_y \times L_z$, (in the *x*, *y*, and *z* directions, respectively) with $L_x = L_y = 10L_s$ and $L_z = 1L_o \approx 1.2R_e$. Various MC moves, including single displacement, reptation, whole chain translation, and swapping of two end blocks, are used to equilibrate the system. The MC moves have been chosen to efficiently sample the configuration space and are not intended to mimic single-molecule motion. We do, however, expect that the sequence of morphologies be qualitatively independent from the details of single-chain motion and are chiefly dictated by the free-energy landscape. Each simulation is run for at least 10^5 MC steps, although for most systems, equilibrium is reached after a much smaller number of MC steps.

Conflict of Interest: The authors declare no competing financial interest.

Acknowledgment. We thank the funding from UW-NSF Nanoscale Science and Engineering Center (NSEC) (DMR 0832760) and the Semiconductor Research Corporation. S.J. thanks the startup support from Changchun Institute of Applied Chemistry, Chinese Academy of Sciences. and the funding from National Natural Science Foundation of China (No. 51173181). M. M. acknowledges financial support by the Volkswagen foundation.

Supporting Information Available: Figure S1: SEM images. This material is available free of charge *via* the Internet at http://pubs.acs.org.

REFERENCES AND NOTES

1. Kim, S. O.; Solak, H. H.; Stoykovich, M. P.; Ferrier, N. J.; de Pablo, J. J.; Nealey, P. F. Epitaxial Self-Assembly of Block Copolymers on Lithographically Defined Nanopatterned Substrates. *Nature* **2003**, *424*, 411–414.
2. Edwards, E. W.; Montague, M. F.; Solak, H. H.; Hawker, C. J.; Nealey, P. F. Precise Control over Molecular Dimensions of Block-Copolymer Domains Using the Interfacial Energy of Chemically Nanopatterned Substrates. *Adv. Mater.* **2004**, *16*, 1315–1319.
3. Edwards, E. W.; Stoykovich, M. P.; Muller, M.; Solak, H. H.; de Pablo, J. J.; Nealey, P. F. Mechanism and Kinetics of Ordering in Diblock Copolymer Thin Films on Chemically Nanopatterned Substrates. *J. Polym. Sci., Part B: Polym. Phys.* **2005**, *43*, 3444–3459.
4. Edwards, E. W.; Muller, M.; Stoykovich, M. P.; Solak, H. H.; de Pablo, J. J.; Nealey, P. F. Dimensions and Shapes of Block Copolymer Domains Assembled on Lithographically Defined Chemically Patterned Substrates. *Macromolecules* **2007**, *40*, 90–96.
5. Welander, A. M.; Kang, H. M.; Stuen, K. O.; Solak, H. H.; Muller, M.; de Pablo, J. J.; Nealey, P. F. Rapid Directed Assembly of Block Copolymer Films at Elevated Temperatures. *Macromolecules* **2008**, *41*, 2759–2761.
6. Stoykovich, M. P.; Muller, M.; Kim, S. O.; Solak, H. H.; Edwards, E. W.; de Pablo, J. J.; Nealey, P. F. Directed Assembly of Block Copolymer Blends into Nonregular Device-Oriented Structures. *Science* **2005**, *308*, 1442–1446.
7. Kang, H.; Craig, G. S. W.; Nealey, P. F. Directed Assembly of Asymmetric Ternary Block Copolymer-Homopolymer Blends Using Symmetric Block Copolymer into Checkerboard Trimming Chemical Pattern. *J. Vac. Sci. Technol., B* **2008**, *26*, 2495–2499.
8. Kang, H.; Detcheverry, F. A.; Mangham, A. N.; Stoykovich, M. P.; Daoulas, K. C.; Hamers, R. J.; Muller, M.; de Pablo, J. J.; Nealey, P. F. Hierarchical Assembly of Nanoparticle Superstructures from Block Copolymer-Nanoparticle Composites. *Phys. Rev. Lett.* **2008**, *100*, 148303.
9. Stoykovich, M. P.; Kang, H.; Daoulas, K. C.; Liu, G.; Liu, C. C.; de Pablo, J. J.; Mueller, M.; Nealey, P. F. Directed Self-Assembly of Block Copolymers for Nanolithography: Fabrication of Isolated Features and Essential Integrated Circuit Geometries. *ACS Nano* **2007**, *1*, 168–175.
10. Ruiz, R.; Dobisz, E.; Albrecht, T. R. Rectangular Patterns Using Block Copolymer Directed Assembly for High Bit Aspect Ratio Patterned Media. *ACS Nano* **2011**, *5*, 79–84.
11. Ji, S. X.; Liu, C. C.; Liu, G. L.; Nealey, P. F. Molecular Transfer Printing Using Block Copolymers. *ACS Nano* **2010**, *4*, 599–609.
12. Liu, G. L.; Thomas, C. S.; Craig, G. S. W.; Nealey, P. F. Integration of Density Multiplication in the Formation of Device-Oriented Structures by Directed Assembly of Block Copolymer-Homopolymer Blends. *Adv. Funct. Mater.* **2010**, *20*, 1251–1257.
13. Ji, S. X.; Nagpal, U.; Liao, W.; Liu, C.-C.; de Pablo, J. J.; Nealey, P. F. Three-Dimensional Directed Assembly of Block Copolymers Together with Two-Dimensional Square and Rectangular Nanolithography. *Adv. Mater.* **2011**, *23*, 3692–3697.
14. Liu, C. C.; Han, E.; Onses, M. S.; Thode, C. J.; Ji, S. X.; Gopalan, P.; Nealey, P. F. Fabrication of Lithographically Defined Chemically Patterned Polymer Brushes and Mats. *Macromolecules* **2011**, *44*, 1876–1885.
15. Ruiz, R.; Kang, H. M.; Detcheverry, F. A.; Dobisz, E.; Kercher, D. S.; Albrecht, T. R.; de Pablo, J. J.; Nealey, P. F. Density Multiplication and Improved Lithography by Directed Block Copolymer Assembly. *Science* **2008**, *321*, 936–939.
16. Bita, I.; Yang, J. K. W.; Jung, Y. S.; Ross, C. A.; Thomas, E. L.; Berggren, K. K. Graphoepitaxy of Self-Assembled Block Copolymers on Two-Dimensional Periodic Patterned Templates. *Science* **2008**, *321*, 939–943.
17. Cheng, J. Y.; Rettner, C. T.; Sanders, D. P.; Kim, H. C.; Hinsberg, W. D. Dense Self-Assembly on Sparse Chemical Patterns: Rectifying and Multiplying Lithographic Patterns Using Block Copolymers. *Adv. Mater.* **2008**, *20*, 3155–3158.
18. Tada, Y.; Akasaka, S.; Takenaka, M.; Yoshida, H.; Ruiz, R.; Dobisz, E.; Hasegawa, H. Nine-Fold Density Multiplication of HCP Lattice Pattern by Directed Self-Assembly of Block Copolymer. *Polymer* **2009**, *50*, 4250–4256.
19. Xiao, S. G.; Yang, X. M.; Park, S. J.; Weller, D.; Russell, T. P. A Novel Approach to Addressable 4 Teradot/in^2 Patterned Media. *Adv. Mater.* **2009**, *21*, 2516–2519.
20. Yang, X. M.; Wan, L.; Xiao, S. G.; Xu, Y. A.; Weller, D. K. Directed Block Copolymer Assembly *versus* Electron Beam Lithography for Bit-Patterned Media with Areal Density of 1 Terabit/inch^2 and Beyond. *ACS Nano* **2009**, *3*, 1844–1858.
21. Hellwig, O.; Bosworth, J. K.; Dobisz, E.; Kercher, D.; Hauet, T.; Zeltzer, G.; Risner-Jamtgaard, J. D.; Yaney, D.; Ruiz, R. Bit Patterned Media Based on Block Copolymer Directed Assembly with Narrow Magnetic Switching Field Distribution. *Appl. Phys. Lett.* **2010**, *96*, 052511.
22. Yang, X. M.; Xu, Y.; Lee, K.; Xiao, S. G.; Ku, D.; Weller, D. Advanced Lithography for Bit Patterned Media. *IEEE Trans. Magn.* **2009**, *45*, 833–838.
23. Albrecht, T. R.; Hellwing, O.; Ruiz, R.; Schabes, M. E.; Terris, B. D.; Wu, X. Z. Bit-Patterned Magnetic Recording: Nanoscale Magnetic Islands for Data Storage. *Nanoscale Magnetic Materials and Applications*; Springer: Berlin, 2009; pp 237−274.
24. Black, C. T.; Ruiz, R.; Breyta, G.; Cheng, J. Y.; Colburn, M. E.; Guarini, K. W.; Kim, H. C.; Zhang, Y. Polymer Self Assembly in Semiconductor Microelectronics. *IBM J. Res. Dev.* **2007**, *51*, 605–633.
25. Park, S. M.; Ravindran, P.; La, Y. H.; Craig, G. S. W.; Ferrier, N. J.; Nealey, P. F. Combinatorial Generation and Replication-Directed Assembly of Complex and Varied Geometries with Thin Films of Diblock Copolymers. *Langmuir* **2007**, *23*, 9037–9045.
26. Dejeu, W. H.; Lambooy, P.; Hamley, I. W.; Vaknin, D.; Pedersen, J. S.; Kjaer, K.; Seyger, R.; Vanhutten, P.; Hadziioannou, G. On the Morphology of a Lamellar Triblock Copolymer Film. *J. Phys. II* **1993**, *3*, 139–146.
27. Matsen, M. W. Bridging and Looping in Multiblock Copolymer Melts. *J. Chem. Phys.* **1995**, *102*, 3884–3887.
28. Matsen, M. W.; Schick, M. Lamellar Phase of a Symmetrical Triblock Copolymer. *Macromolecules* **1994**, *27*, 187–192.
29. Matsen, M. W.; Thompson, R. B. Equilibrium Behavior of Symmetric ABA Triblock Copolymer Melts. *J. Chem. Phys.* **1999**, *111*, 7139–7164.

30. Mayes, A. M.; Delacruz, M. O. Microphase Separation in Multiblock Copolymer Melts. *J. Chem. Phys.* **1989**, *91*, 7228–7235.
31. Milner, S. T. Chain Architecture and Asymmetry in Copolymer Microphases. *Macromolecules* **1994**, *27*, 2333–2335.
32. Gehlsen, M. D.; Almdal, K.; Bates, F. S. Order−Disorder Transition-Diblock *versus* Triblock Copolymers. *Macromolecules* **1992**, *25*, 939–943.
33. Mai, S. M.; Mingvanish, W.; Turner, S. C.; Chaibundit, C.; Fairclough, J. P. A.; Heatley, F.; Matsen, M. W.; Ryan, A. J.; Booth, C. Microphase-Separation Behavior of Triblock Copolymer Melts. Comparison with Diblock Copolymer Melts. *Macromolecules* **2000**, *33*, 5124–5130.
34. Watanabe, H. Slow Dielectric-Relaxation of a Styrene−Isoprene−Styrene Triblock Copolymer with Dipole Inversion in the Middle Block - A Challenge to a Loop-Bridge Problem. *Macromolecules* **1995**, *28*, 5006–5011.
35. Helfand, E.; Wasserman, Z. R. Block Copolymer Theory 0.4. Narrow Interphase Approximation. *Macromolecules* **1976**, *9*, 879–888.
36. Leibler, L. Theory of Microphase Separation in Block Copolymers. *Macromolecules* **1980**, *13*, 1602–1617.
37. Mansky, P.; Liu, Y.; Huang, E.; Russell, T. P.; Hawker, C. J. Controlling Polymer−Surface Interactions with Random Copolymer Brushes. *Science* **1997**, *275*, 1458–1460.
38. Ryu, D. Y.; Shin, K.; Drockenmuller, E.; Hawker, C. J.; Russell, T. P. A Generalized Approach to the Modification of Solid Surfaces. *Science* **2005**, *308*, 236–239.
39. In, I.; La, Y. H.; Park, S. M.; Nealey, P. F.; Gopalan, P. Side-Chain-Grafted Random Copolymer Brushes as Neutral Surfaces for Controlling the Orientation of Block Copolymer Microdomains in Thin Films. *Langmuir* **2006**, *22*, 7855–7860.
40. Ji, S.; Liu, C. C.; Son, J. G.; Gotrik, K.; Craig, G. S. W.; Gopalan, P.; Himpsel, F. J.; Char, K.; Nealey, P. F. Generalization of the Use of Random Copolymers To Control the Wetting Behavior of Block Copolymer Films. *Macromolecules* **2008**, *41*, 9098–9103.
41. Ji, S. X.; Liu, G. L.; Zheng, F.; Craig, G. S. W.; Himpsel, F. J.; Nealey, P. F. Preparation of Neutral Wetting Brushes for Block Copolymer Films from Homopolymer Blends. *Adv. Mater.* **2008**, *20*, 3054–3060.
42. Han, E.; Stuen, K. O.; La, Y. H.; Nealey, P. F.; Gopalan, P. Effect of Composition of Substrate-Modifying Random Copolymers on the Orientation of Symmetric and Asymmetric Diblock Copolymer Domains. *Macromolecules* **2008**, *41*, 9090–9097.
43. Bates, C. M.; Strahan, J. R.; Santos, L. J.; Mueller, B. K.; Bamgbade, B. O.; Lee, J. A.; Katzenstein, J. M.; Ellison, C. J.; Willson, C. G. Polymeric Cross-Linked Surface Treatments for Controlling Block Copolymer Orientation in Thin Films. *Langmuir* **2011**, *27*, 2000–2006.
44. Ji, S. X.; Liao, W.; Nealey, P. F. Block Cooligomers: A Generalized Approach to Controlling the Wetting Behavior of Block Copolymer Thin Films. *Macromolecules* **2010**, *43*, 6919–6922.
45. Ji, S. X.; Liu, C. C.; Liao, W.; Fenske, A. L.; Craig, G. S. W.; Nealey, P. F. Domain Orientation and Grain Coarsening in Cylinder-Forming Poly(styrene-*b*-methyl methacrylate) Films. *Macromolecules* **2011**, *44*, 4291–4300.
46. Wu, L. F.; Cochran, E. W.; Lodge, T. P.; Bates, F. S. Consequences of Block Number on the Order−Disorder Transition and Viscoelastic Properties of Linear (AB)(*n*) Multiblock Copolymers. *Macromolecules* **2004**, *37*, 3360–3368.
47. Daoulas, K. C.; Muller, M.; Stoykovich, M. P.; Kang, H.; de Pablo, J. J.; Nealey, P. F. Directed Copolymer Assembly on Chemical Substrate Patterns: A Phenomenological and Single-Chain-in-Mean-Field Simulations Study of the Influence of Roughness in the Substrate Pattern. *Langmuir* **2008**, *24*, 1284–1295.
48. Daoulas, K. C.; Muller, M.; Stoykovich, M. P.; Papakonstantopoulos, Y. J.; de Pablo, J. J.; Nealey, P. F.; Park, S. M.; Solak, H. H. Directed Assembly of Copolymer Materials on Patterned Substrates: Balance of Simple Symmetries in Complex Structures. *J. Polym. Sci., Part B: Polym. Phys.* **2006**, *44*, 2589–2564.
49. Detcheverry, F. A.; Pike, D. Q.; Nagpal, U.; Nealey, P. F.; de Pablo, J. J. Theoretically Informed Coarse Grain Simulations of Block Copolymer Melts: Method and Applications. *Soft Matter* **2009**, *5*, 4858–4865.
50. Detcheverry, F. A.; Pike, D. Q.; Nealey, P. F.; Muller, M.; de Pablo, J. J. Monte Carlo Simulation of Coarse Grain Polymeric Systems. *Phys. Rev. Lett.* **2009**, *102*, 197801.
51. Lipowsky, R.; Dobereiner, H. G.; Hiergeist, C.; Indrani, V. Membrane Curvature Induced by Polymers and Colloids. *Physica A* **1998**, *249*, 536–543.
52. Stoykovich, M. P.; Edwards, E. W.; Solak, H. H.; Nealey, P. F. Phase Behavior of Symmetric Ternary Block Copolymer-Homopolymer Blends in Thin Films and on Chemically Patterned Surfaces. *Phys. Rev. Lett.* **2006**, *97*, 147802.
53. Thompson, R. B.; Rasmussen, K. O.; Lookman, T. Elastic Moduli of Multiblock Copolymers in the Lamellar Phase. *J. Chem. Phys.* **2004**, *120*, 3990–3996.
54. Daoulas, K. C.; Muller, M. Single Chain in Mean Field Simulations: Quasi-instantaneous Field Approximation and Quantitative Comparison with Monte Carlo Simulations. *J. Chem. Phys.* **2006**, *125*, 184904.
55. Soga, K. G.; Zuckermann, M. J.; Guo, H. Binary Polymer Brush in a Solvent. *Macromolecules* **1996**, *29*, 1998–2005.
56. Pike, D. Q.; Detcheverry, F. A.; Muller, M.; de Pablo, J. J. Theoretically Informed Coarse Grain Simulations of Polymeric Systems. *J. Chem. Phys.* **2009**, *131*, 084903.
57. Detcheverry, F. A.; Liu, G. L.; Nealey, P. F.; de Pablo, J. J. Interpolation in the Directed Assembly of Block Copolymers on Nanopatterned Substrates: Simulation and Experiments. *Macromolecules* **2010**, *43*, 3446–3454.
58. Muller, M.; Daoulas, K. C. Calculating the Free Energy of Self-Assembled Structures by Thermodynamic Integration. *J. Chem. Phys.* **2008**, *128*, 024903.
59. Muller, M.; Daoulas, K. C.; Norizoe, Y. Computing Free Energies of Interfaces in Self-Assembling Systems. *Phys. Chem. Chem. Phys.* **2009**, *11*, 2087–2097.